Influence of Epitaxial Structure in the Noise Figure of AlGaN/GaN HEMTs

Christopher Sanabria, *Student Member, IEEE*, Hongtao Xu, *Student Member, IEEE*, Tomás Palacios, *Student Member, IEEE*, Arpan Chakraborty, Sten Heikman, Umesh K. Mishra, *Fellow, IEEE*, and Robert A. York, *Senior Member, IEEE*

***Abstract*—The effect of noise figure of different AlGaN/GaN high electron-mobility transistor (HEMT) epitaxy structures is reported. The addition of a thin AlN layer between the barrier and channel gives better performance at biasings other than the best for minimum noise figure. However, varying Al composition in the HEMT barrier does not change the noise performance, contrary to a 2003 study by Lu *et al.* The measurements are checked with both the Pospieszalski and van der Ziel (Pucel) models. The models are used on six different samples, helping to reinforce the measurements and showing the strengths and weaknesses of each.**

***Index Terms*—AlGaN, GaN, high electron-mobility transistor (HEMT), noise figure, Pospieszalski, Pucel, van der Ziel.**

I. Introduction

ALMOST ANY communication system will have to address signal amplification and noise. In such a system, a gain stage is designed to maximize gain while minimizing the amount of noise it adds. This makes figures-of-merits, such as noise figure, important when choosing a device and a material to integrate the device upon. In developing an integrated solution, there are many material systems to work in. Silicon, GaAs, and InP are more common choices.

GaN is presenting itself as a new and attractive option. The biggest benefit is for power amplification. GaN high electron-mobility transistors (HEMTs) have breakdown voltages in excess of 100 V. This eliminates the need for protection circuitry, such as in a front-end receiver, making a GaN-based design less complex and lower noise [2]. In the Ka-band, GaN is currently the only solid-state contender for high-power applications, again, because of its large breakdown voltage.

GaN also has respectable electron mobility (μ) and a high peak electron velocity, thus, it is useful at high frequencies. Since these values translate into a good unity current gain (f_t) and maximum frequency of oscillation ($f_{\max}$), it also performs well for noise. Table I presents a comparison of noise figures and their measurement frequencies for HEMTs in several solid-state technologies including GaN, GaAs, Si, and InP. The best noise performers are In-related materials. The other technologies perform similarly, including GaN.

TABLE I
COMPARISON OF MINIMUM NOISE FIGURES FOR THE STATE-OF-THE-ART IN VARIOUS MATERIAL STRUCTURES FOR HEMTs. DEVICE GATE LENGTH, MINIMUM NOISE FIGURE, FREQUENCY OF MEASUREMENT, COMMENTS ABOUT THE DATA, AND REFERENCE ARE LISTED, RESPECTIVELY. ALL MEASUREMENTS ARE AT ROOM TEMPERATURE

L_g [μm]	Nf_{min} [dB]	Freq. [GHz]	Note	Ref.
GaN HEMTs				
0.15	0.6	10	SiC substrate	[6]
0.15	0.75	10	SiC substrate	[3]
0.18	1.1	18	Sapphire substrate	[1]
0.25	0.8	10	SiC substrate,from graph	[7]
0.25	1.05	18	SiC substrate,from graph	[7]
0.25	1.04	10	Sapphire substrate	[5]
0.25	1.06	10	SiC substrate	[4]
0.25	1.9	10	SiC substrate	[9]
GaAs HEMTs				
0.1	0.3	10	from graph	[9]
0.1	0.51	18		[10]
0.1	1.9	40		[10]
0.25	0.7	18		[10]
Si/SiGe HEMTs				
0.1	1.6	10	from graph, pads de-emb.	[17]
AlGaAs/ InGaAs on GaAs HEMTs				
0.13	0.31	12	pHEMT	[11]
0.13	0.45	18	pHEMT	[11]
0.15	0.24	12	mHEMT	[12]
0.15	0.61	36	mHEMT	[12]
InGaAs/ InAlAs on GaAs HEMTs				
0.1	0.25	12		[13]
InAlAs/ InGaAs on InP HEMTs				
0.1	0.8	60		[14]
0.15	0.4	10		[15]
0.2	0.48	10		[16]
0.2	0.8	26		[16]

Having minimum noise figures ($\mathrm{Nf}_{\min}$) less than 1 dB throughout the X-band [3] and much higher power densities [4] means AlGaN/GaN HEMTs show promise for low-noise microwave applications. While GaAs-based HEMTs might show marginally better noise figures (1/10 or 2/10 of a decibel), GaN material growth and processing are not mature, and improvements in performance are expected.

Only in the last few years have papers been published on microwave noise in GaN HEMTs. The first to do measurements were Ping *et al.* in January 2000. The resulting $\mathrm{Nf}_{\min}$ for 0.25-μm gate-length devices was 0.77 dB at 5 GHz and 1.06 dB at 10 GHz [5], and is comparable to other later results, as shown in Table I. They also claimed comparable noise figures

Manuscript received April 18, 2004; revised July 28, 2004. This work was supported in part by the Office of Naval Research under Contract N00014-01-0764.

The authors are with the Electrical and Computer Engineering Department, University of California at Santa Barbara, Santa Barbara, CA 93106 USA (e-mail: sanabria@ece.ucsb.edu).

Digital Object Identifier 10.1109/TMTT.2004.840578

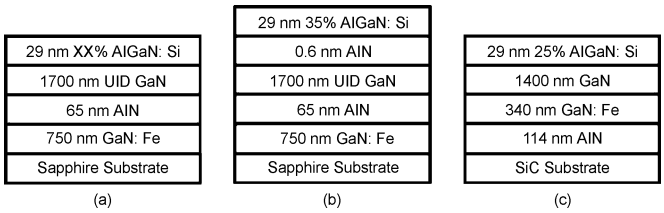

Fig. 1. Cross section of the material structure for: (a) samples with varying aluminum mole fraction, (b) sample with AlN interlayer, and (c) SiC substrate sample.

to GaAs HEMTs and metal–semiconductor field-effect transistors. Moon *et al.* showed that, at a very low-biasing, such as $V_{\rm ds}$ 1 V, noise figures were similar to low-biased GaAs devices [2]. In 2003, Lu *et al.* varied the aluminum mole fraction of the AlGaN barrier to see if it changed the noise figure, finding that higher Al percentage gave a better noise figure [1]. A few other papers have presented standard noise measurements, most already summarized in Table I [1], [2], [5]–[17].

Here, we will study changes in the HEMT epitaxy to see how it affects the noise performance. Four samples with identical structure, except for varying aluminum mole fraction in the AlGaN barrier, are compared. Unlike an earlier aluminum composition study [1], all samples showed the same $\rm Nf_{min}$ against frequency and current. We then present, for the first time, the effect of a very thin aluminum nitride (AlN) layer between the AlGaN and GaN on noise performance. The addition of the AlN layer increases the channel mobility and the two-dimensional electron gas (2-DEG) density as shown by Shen *et al.* [18]. It causes a favorable difference in the $\rm Nf_{min}$ as well. Finally, we verify these results with two transistor noise models, Pospieszalski and van der Ziel (sometimes seen in the Pucel model formulation in the literature). The models are applied to six samples and simulated in Agilent's Advanced Design System (ADS) software. Using so many samples allows for comparison with the measurements to see how well each model performs.

II. Device Structure and Device Processing

The device structures were grown by metal–organic chemical vapor deposition (MOCVD) on both c-plane sapphire and c-plane 4H-SiC substrates. The epitaxial structures of the samples appear in Fig. 1. Four of them, represented in Fig. 1(a), consisted of a GaN nucleation layer followed by a semi-insulating Fe-doped GaN buffer layer, and capped by a 29-nm $\rm Al_xGa_{1-x}N$ layer. Four different Al compositions (15%, 25%, 27%, and 35%) were constructed with this template. In another sample, shown in Fig. 1(b), a 0.6-nm AlN layer was included between the 29-nm $\rm Al_{0.35}Ga_{0.65}N$ layer and GaN channel. The epitaxial structure of the sample grown on SiC substrate, shown in Fig. 1(c), consisted of an AlN nucleation layer followed by a semi-insulating Fe-doped GaN buffer layer and was capped by a 29-nm $\rm Al_{0.35}Ga_{0.65}N$ layer.

The electron mobility and sheet charge concentration from Hall measurements for the samples are in Table II. All samples were identically processed. Source and drain ohmic contacts were created with Ti/Al/Ni/Au electron beam evaporation and rapid thermal annealed at 870 °C for 30 s. Contact resistance for each sample is also presented in Table II. Device isolation was achieved by reactive ion etching (RIE) in $\rm Cl_2$. Stepper photolithography Ni/Au/Ni gates were electron beam evaporated with a nominal gate length of 0.7 μm. $\rm SiN_x$ passivation was achieved with plasma-enhanced chemical vapor deposition. All devices in this paper have a gatewidth of 2×75 μm, a gate–source spacing of 0.7 μm, and a gate–drain spacing of 2 μm. The pads are a coplanar waveguide (CPW) layout.

TABLE II
Data From Hall Measurements (Sheet Charge Concentration, and Mobility), S-Parameter Measurements (Best f_t and $f_{\rm max}$ for the Device), and Transmission-Line Matrix (TLM) Measurements (Sheet and Contact Resistances)

Al mole fraction	15%	25%	25% SiC	27%	35%	35% w/AlN
n [10^{12} cm^{-2}]	4.30	8.60		11.5	13.0	14.2
μ@300 K [cm^2/Vs]	1565	1460		1211	1122	1690
best f_t [GHz]	25.5	19.3	23.2	23.3	23.8	24.1
best f_{max} [GHz]	46.6	45.8	51.5	50.5	49.6	46.3
R_{sheet} [Ω/sq.]	878	468	438	389	334	258
$R_{contact}$ [Ω mm]	0.92	0.6	0.47	0.33	0.41	0.62

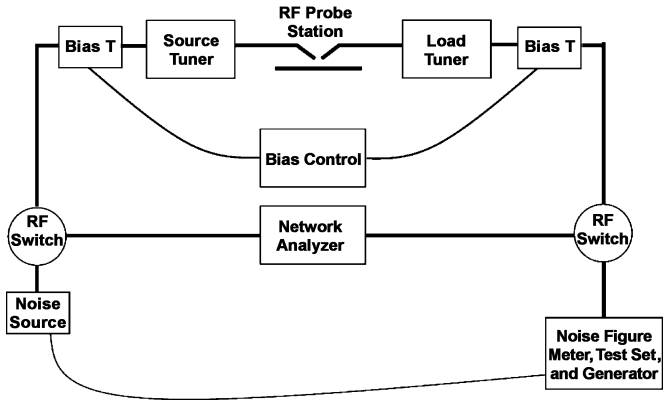

Fig. 2. Schematic of the source–pull noise-figure measurement system for noise or S-parameter measurements.

III. Procedure

All measurements were performed on-wafer with Cascade-Microtech ACP40 ground–signal–ground CPW probes. S-parameters were measured with an HP 8722D vector network analyzer (VNA) at several different device biases. From this, the frequencies for f_t and $f_{\rm max}$ were collected. The biasing was such as to find *independently* the best possible f_t and $f_{\rm max}$ for each device, which are presented in Table II.

Noise measurements were performed with a source–pull noise-figure system. A schematic is presented in Fig. 2. Noise was measured with an HP 8970S noise-figure meter with an Agilent 346B noise source. The varying input impedance is generated by a Maury Microwave MT982A02 mechanical motorized tuner. The load tuner was set to 50 Ω. A Maury Microwave MT998C RF switch changes between noise and S-parameter measurements. An HP 8722D measures S-parameters. The bias was set automatically by an HP 6625A

System dc power supply. All components were controlled by a general-purpose interface bus (GPIB) by a proprietary Maury Microwave software program. The system was checked with an in-house fabricated CPW attenuator on GaN. Error in noise figure is ± 0.1 dB.

IV. Measurements and Analysis

It is well known that f_t and $f_{\max}$ have the largest influence on noise figure [19]. It is, therefore, imperative when comparing devices from different samples that they have similar f_t and $f_{\max}$. From each sample, two typical devices with similar f_t and $f_{\max}$ were used for all measurements. In the graphs that follow, only the first device from each sample is plotted for clarity. The second device from each sample was measured as a check on validity and only reinforces the data presented.

The dc bias for lowest $\mathrm{Nf}_{\min}$ was found for each device. This also helps give a fair comparison among the different devices. The noise bias was found by setting V_{gs} close to pinchoff, then varying V_{ds} for the best $\mathrm{Nf}_{\min}$. With V_{ds} set to this new value as a constant, I_{ds} was swept in a coarse 5-mA sweep and then a 1-mA fine sweep to find the bias. It is worth noting that the optimal bias for noise, i.e., f_t, and $f_{\max}$ are not the same. The best bias for noise was found to typically be V_{ds} of 4–5 V and an I_{ds} approximately 10–20 mA. For f_t and $f_{\max}$, the optimal bias for all devices was typically V_{ds} 7 V and a I_{ds} between 20–30 mA, being higher for $f_{\max}$. The $\mathrm{Nf}_{\min}$ against the drain–source voltage is relatively flat [7], thus, plots of it are not included.

A. Varying Aluminum Composition Study

Measurements of the four samples structured as shown in Fig. 1(a) are plotted in Fig. 3(a)–(d). Here, we see the four noise parameters and the gain: the $\mathrm{Nf}_{\min}$ in (a), Γ_{opt}: the *complex* optimum source reflection coefficient (magnitude and phase) in (b), r_n: the normalized (to 50 Ω) noise resistance in (c), and G_a: the associated gain in (d), respectively. All are plotted against frequency for the 15%, 25%, 27%, and 35% aluminum mole fraction devices. Connecting lines are not a model and are added only as a visual aid to distinguish the data series. Each device as biased for lowest noise performance.

The $\mathrm{Nf}_{\min}$ increases from approximately 1 to 2.3 dB over the 4–12-GHz measurements for the devices. This linear trend is common for noise measurements versus frequency. The magnitude of the source reflection coefficient drops from just over 0.8 at 4 GHz to 0.6 at 12 GHz, while the phase of the reflection coefficient increases almost linearly from approximately 18° to 55° over the same range. The overlap of the measurements is very good. The normalized noise resistance fluctuates in the range from approximately 0.7 to 0.9. It is relatively flat, which is an indicator of stability and accuracy in the noise measurements. The associated gains drop off from 15 to 8 dB with increasing frequency at a near −20-dB/decade slope. Differences in associated gain between the devices in Fig. 3(d) are as large as 1.5 dB. While the gain can affect the noise performance, as seen later in (1), the noise figures are still very close in value for all four devices.

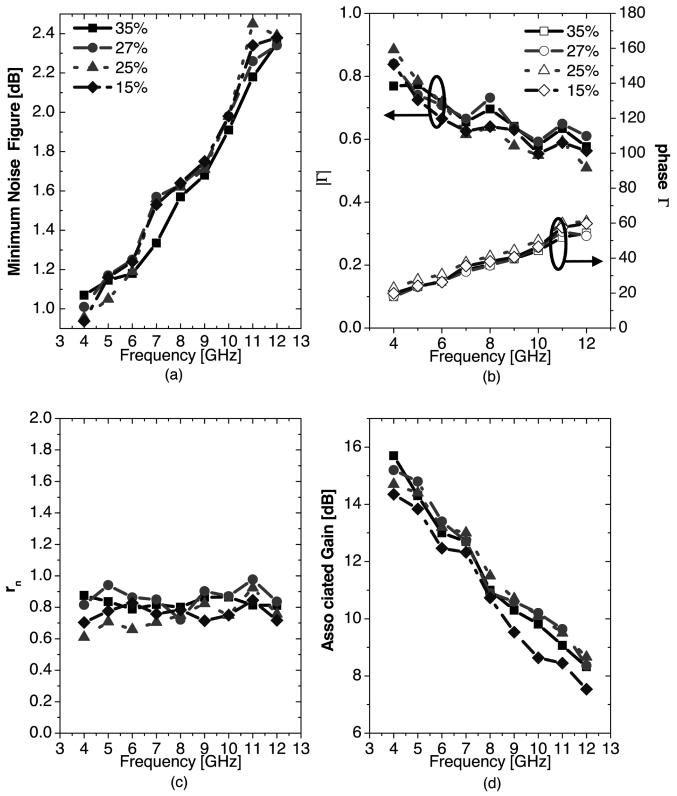

Fig. 3. Noise parameters of four devices from similar samples with varying aluminum mole fraction, each biased for lowest noise (as in Table IV). (a) Minimum noise figure. (b) Optimum source impedance (magnitude and phase). (c) Noise resistance (normalized by 50 Ω). (d) Associated gain.

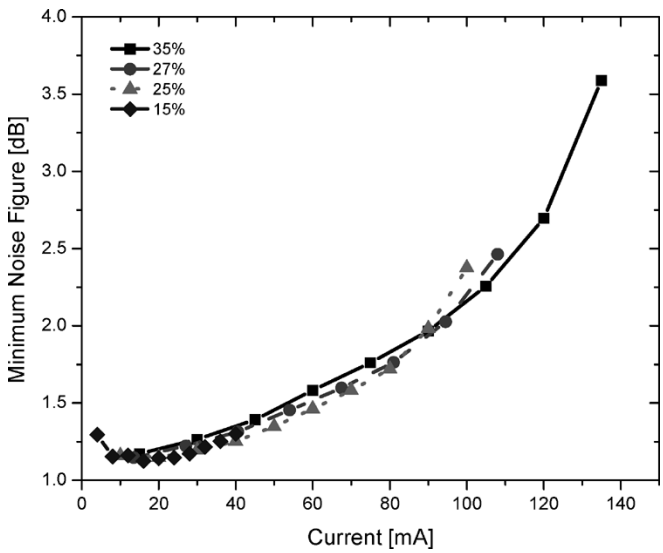

Fig. 4. Noise figure versus I_{ds} of four devices with varying aluminum mole fraction. Measurements made at 5 GHz with V_{ds} of each device as found in Table IV.

In Fig. 4, we see the same four devices with their $\mathrm{Nf}_{\min}$ plotted against the drain–source current. Each device is plotted up to its maximum current. The measurement frequency is 5 GHz and the drain–source biasings are 4, 4, 4, and 5 V for the 15%, 25%, 27%, and 35% devices, respectively. The overlap

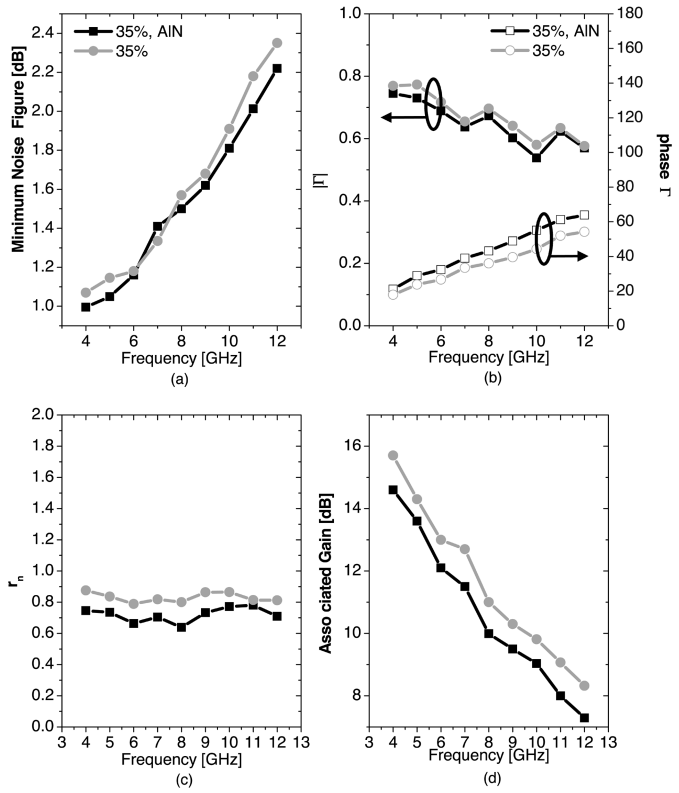

Fig. 5. Noise parameters of similar devices with and without an AlN layer, each biased for lowest noise (see Table IV). (a) Minimum noise figure. (b) Optimum source impedance. (c) Noise resistance. (d) Associated gain.

of the four devices' measurements is excellent. Figs. 3 and 4 present a convincing argument that Al composition does not effect the $\mathrm{Nf}_{\min}$, unlike what was found in [1]. Changing the Al composition will slightly change the barrier height in the band diagram, the total charge, and the maximum current (I_{dss}). As shown by modeling in Section V, these changes do not significantly change the small-signal parameters or the noise parameters. Presented in Section IV-B is a parameter that does change the noise figure.

B. With and Without AlN Layer

Figs. 5 and 6 show a comparison of noise parameter measurements for a device with and without a very thin AlN layer between the channel and AlGaN barrier. In Fig. 5, we again see $\mathrm{Nf}_{\min}$, optimum source reflection coefficient (magnitude and phase), noise resistance, and associated gain against frequency. In Fig. 6, the $\mathrm{Nf}_{\min}$ is plotted against drain–source current with the AlN layer device biased at V_{ds} 4 V and the device without the layer at V_{ds} 5 V. The measurement frequency is again 5 GHz. For each bias used for the noise data points, f_t and $f_{\max}$ were measured and also appear in Fig. 6.

Many of the same trends are seen here as in the previous plots, with similar values and shapes. The difference is that the device with the AlN layer has slightly less gain, a smaller noise resistance, and smaller optimum source reflection-coefficient phase over the entire 4–12-GHz frequency range than the device without an AlN thin layer. The difference in $\mathrm{Nf}_{\min}$ against

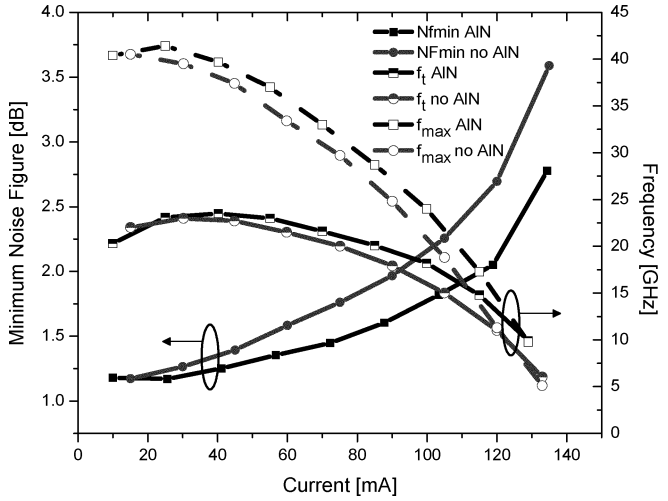

Fig. 6. Noise figure (f_t and $f_{\max}$) versus I_{ds} of devices with and without an aluminum–nitride layer. Measurements made at 5 GHz with V_{ds} that gave the lowest noise measurements.

frequency is never more than 0.15 dB, and can be judged a good match.

Observing Fig. 6, a difference in noise figure against current is evident. In this plot, the AlN layer is lower in $\mathrm{Nf}_{\min}$ as the current increases. Both devices are approximately the same $\mathrm{Nf}_{\min}$ until the current is greater than 20 mA when the device without the AlN layer increases its $\mathrm{Nf}_{\min}$ faster with increasing current. At 135 mA, this difference is greater than 0.8 dB. $f_{\max}$ ultimately determines the power gain for the device, which factors directly into the noise-figure definition as

$$F = \frac{\left(\frac{S}{N}\right)_{\mathrm{in}}}{\left(\frac{S}{N}\right)_{\mathrm{out}}} = \frac{N_{\mathrm{in}}G + N_a}{N_{\mathrm{in}}G} = 1 + \frac{N_a}{N_{\mathrm{in}}G} \tag{1}$$

were F is the noise figure, S is the signal coming in or going out of the device, N is the noise coming in or going out of the device, G is the gain, and N_a is the noise added by the device. The gain is defined as

$$G = \frac{S_{\mathrm{out}}}{S_{\mathrm{in}}} \tag{2}$$

and the noise out as

$$N_{\mathrm{out}} = N_a + GN_{\mathrm{in}}. \tag{3}$$

A larger gain for a given amount of device noise means a lower noise figure. In Fig. 6, we see that the device with the AlN layer maintains a higher f_t and $f_{\max}$ at all currents above 20 mA. Note that the intersection of the two devices' $f_{\max}$ is the bias for each device's best noise performance and is where their $\mathrm{Nf}_{\min}$ is the same. The AlN provides better confinement of the 2DEG at higher currents. This causes a better f_t and $f_{\max}$, as seen in Fig. 6, and, thus, better noise performance.

V. Modeling

To confirm the results, and to test the accuracy of two noise models, the devices were modeled with the van der Ziel and

TABLE III
EXTRACTED INTRINSIC AND EXTRINSIC SMALL-SIGNAL PARAMETERS WITH EACH DEVICE BIASED AS IN TABLE IV

Al mole fraction	15%	25%	25% SiC	27%	35%	35% w/AlN
R_i [Ω]	6.2	8.24	8.86	9.23	8.23	4.07
R_{ds} [Ω]	577	588	622	562	833	627
R_{gd} [Ω]	75.7	287	238	96	96.2	33.4
C_{gd} [fF]	19	19.1	13.5	20.6	18.7	29.9
C_{ds} [fF]	2.97	2.33	1.34	2.34	1.66	1.13
C_{gs} [pF]	0.23	0.27	0.22	0.19	0.19	0.215
g_m [mS]	34.1	37	33.2	33	30.5	34.9
τ [ps]	1.2	2.25	2.6	2	2.25	2.03
R_s [Ω]	10.2	6.18	5.19	4.04	4.31	5.30
R_d [Ω]	17.9	10.24	8.99	7.41	7.20	7.54
R_g [Ω]	3.03	3.03	3.03	3.03	3.03	3.03
L_s [pH]	12	12	12	12	12	12
L_d [pH]	22.3	22.3	22.3	22.3	22.3	22.3
L_g [pH]	45.6	45.6	45.6	45.6	45.6	45.6
C_{pgs} [fF]	1.38	1.38	1.38	1.38	1.38	1.38
C_{pds} [fF]	29.6	29.6	29.6	29.6	29.6	29.6
C_{pgd} [fF]	5.4	5.4	5.4	5.4	5.4	5.4

Pospieszalski methods. Noise modeling of transistors usually follows the two-port formulation of Rothe and Dahlke [20]. The Pospieszalski and van der Ziel models are based on this formulation. These models use four measured noise parameters [$\mathrm{Nf}_{\min}$, R_n, and complex Γ_{opt} (magnitude and phase)] at one frequency and the S-parameters of a device to predict the noise at other frequencies and different source reflection coefficients.

S-parameters were taken at the best biases for noise performance for each device. Using extrinsic and intrinsic small-signal parameter extraction techniques, as found in [19], [21], [22], the small-signal circuit parameters were determined in ADS and an equivalent circuit constructed for each device. These parameters are listed in Table III with the bias for each device found in Table IV. The top half of the table is the intrinsic parameters and the bottom half is the extrinsic parameters. Smith chart plots of the S-parameters from this modeling are verified against measured data in Fig. 7. This comparison for the 35% aluminum mole fraction sample of modeled and measured S-parameters was typical and shows excellent agreement.

Another popular model is the Fukui model, but it is not considered here because it is based on finding a fitting parameter from measurements and has been shown to not work well above ∼26 GHz. The reason for this is that the model does not take into account the feedback capacitance C_{gd} and higher order frequency terms [23].

In the van der Ziel model, there is an equivalent noise source at the gate i_g and the drain i_d, as shown in Fig. 8(a). These sources, correlated with the complex variable C, generate all the noise that would be found in the intrinsic device. van der Ziel's formulation was extended by Pucel and Haus. The Pucel formulation would represent van der Ziel's in terms of three parameters, P, R, and C [24]. The extrinsic parameter parasitics still generate thermal noise that increase the noise figure [25]. Hillbrand and Russer created a method of extracting the noise

TABLE IV
MEASURED NOISE PARAMETERS, VALUES FROM POSPIESZALSKI AND VAN DER ZIEL MODELS FOR ALL SAMPLES. ALL DEVICES HAVE A NOMINAL GATE LENGTH OF 0.7 μm AND GATEWIDTH OF 150 μm. ALL DATA IS AT A FREQUENCY OF 5 GHz

Measurements						
Al mole fraction	15%	25%	25% SiC	27%	35%	35% w/AlN
$\mathrm{Nf}_{\min}$ [dB]	1.14	1.13	1.1	1.16	1.15	1.18
r_n	0.77	0.70	0.64	0.83	0.79	0.723
$\lvert\Gamma_{\mathrm{opt}}\rvert$	0.72	0.71	0.74	0.77	0.76	0.733
$\angle\,\Gamma_{\mathrm{opt}}$ [deg.]	20.5	21.3	23.2	19.8	19.5	23.9
Associated Gain [dB]	14	13.7	14.6	14.3	14	12.7
I_{ds} @ $\mathrm{Nf}_{\min}$ [mA]	20	13	10	19	11	10
V_{ds} @ $\mathrm{Nf}_{\min}$ [V]	4	4	7	4	5	4
f_t @ $\mathrm{Nf}_{\min}$ [GHz]	19.7	19.4	21.4	23.3	22.3	21.3
$f_{\max}$ @ $\mathrm{Nf}_{\min}$ [GHz]	30.2	33.6	39	42.9	43.7	40.4
Pospieszalski Model						
$\mathrm{Nf}_{\min}$ modeled [dB]	1.18	1.1	1.1	1.04	1.07	1.03
r_n modeled	0.74	0.59	0.72	0.81	0.83	0.721
$\lvert\Gamma_{\mathrm{opt}}\rvert$ modeled	0.70	0.66	0.71	0.74	0.74	0.72
$\angle\,\Gamma_{\mathrm{opt}}$ modeled [deg.]	25.7	27.3	26.3	22.7	22.3	26.9
T_g [K]	607	292	250	358	462	988
T_d [K]	3445	3018	3893	3469	4454	3966
van der Ziel Model (using Sungjae Lee Formulation)						
$\mathrm{Nf}_{\min}$ modeled [dB]	1.23	1.3	1.21	1.28	1.25	1.33
r_n modeled	1.21	0.98	0.83	1.04	0.97	0.95
$\lvert\Gamma_{\mathrm{opt}}\rvert$ modeled	0.80	0.75	0.77	0.79	0.78	0.766
$\angle\,\Gamma_{\mathrm{opt}}$ modeled [deg.]	19.2	21.0	22.5	19.6	19.2	23.6
$\langle\lvert i_g\rvert^2\rangle$ [10^{-24} A^2/Hz]	7.05	12.0	3.55	7.09	7.23	6.74
$\langle\lvert i_d\rvert^2\rangle$ [10^{-22} A^2/Hz]	4.56	5.60	4.14	5.93	4.79	5.36
$\lvert C\rvert$	0.80	0.79	0.82	0.80	0.75	0.739
$\angle\,C$	103	101	129	114	114	118

correlation matrices from noise and s-parameter measurements to the noise parameters [26]. This analysis was recently put into a convenient form by Lee *et al.*, which is easy to enter into a computer program [27], [28].

Pospieszalski's model gives two parameters from the measured noise parameters: T_g, a gate noise temperature, and T_d, a drain noise temperature. To predict the noise figure in a small-signal model for a transistor, only the channel and drain–source resistances generate noise at these elevated temperatures, as shown in Fig. 8(b). These two sources of noise are uncorrelated. The equations to find these two parameters are found in [29].

The initial parameters of Pospieszalski and van der Ziel models must be found from measurements at one frequency, allowing prediction at other frequencies. Currently there does not exist an accurate model to go directly from the s-parameters to the model parameters.

Both models have been implemented in ADS, which calculates the models' noise parameters from the noise measurements and small-signal parameters, and then simulates for noise. The results are presented in Table IV, which is divided into three sections. The top section lists measurements, at 5 GHz, of the noise parameters, f_t and $f_{\max}$ with the biasing conditions. Notice the agreement of the noise parameters for all samples. This supports the claim that all the different samples are capable of having the same best $\mathrm{Nf}_{\min}$. In the middle section of Table IV are listed the two noise temperatures found from the Pospieszalski model

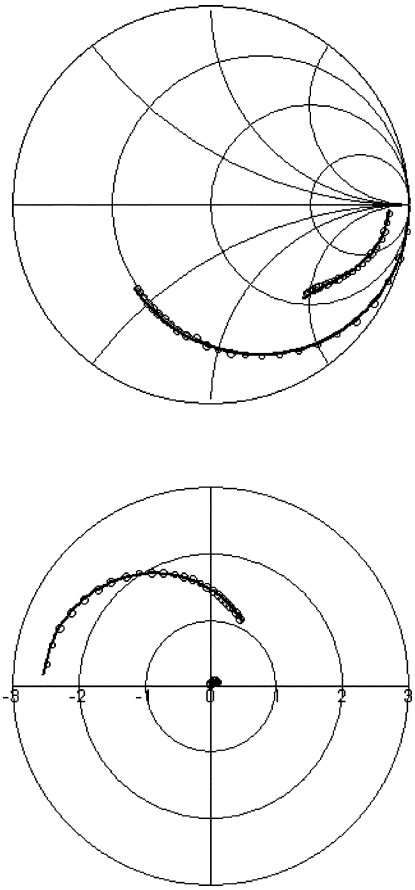

Fig. 7. Measured (circles) and modeled (line) S-parameters showing verification of small-signal modeling. Shown is the 35% aluminum device without an AlN layer biased at $V_{\rm ds}$ 5 V and $I_{\rm ds}$ 11 mA. Frequency range is from 500 MHz to 25 GHz.

along with the noise parameters the model predicts when simulated in ADS. The bottom section of Table IV includes the gate and drain noise currents, the complex correlation coefficient for the van der Ziel model, and the noise parameters the model predicted when simulated in ADS. The comparisons made in the following discussion at 5 GHz apply for the models over the entire 4–12-GHz measurement range.

The Pospieszalski model gave a drain temperature value that averaged 3700 K and a gate temperature of 493 K. The listed noise figures are within 0.12 dB of the measured values, a good agreement, as the expected error in the measurements was $\pm$0.1 dB. The modeled reflection coefficient is also in very good agreement with typically a 0.03 error from the measured value. The modeled noise resistance for the samples is off $\pm$0.1. The optimum source reflection coefficient phase is off by a few degrees.

The van der Ziel model also did well in predicting the measured $\rm Nf_{min}$ usually being approximately 0.1 dB too high. The modeled phase was excellent, usually being less than 1° from measurements. The modeled reflection coefficient magnitude also corresponds well to the data being only $\sim$0.04 in excess. The modeled noise resistance, though, was not correct, as it was from 0.2 to 0.5 over the measured value. Typical drain current noise was 5×10^{-22} A^2/Hz and gate current noise of 7×10^{-24} A^2/Hz.

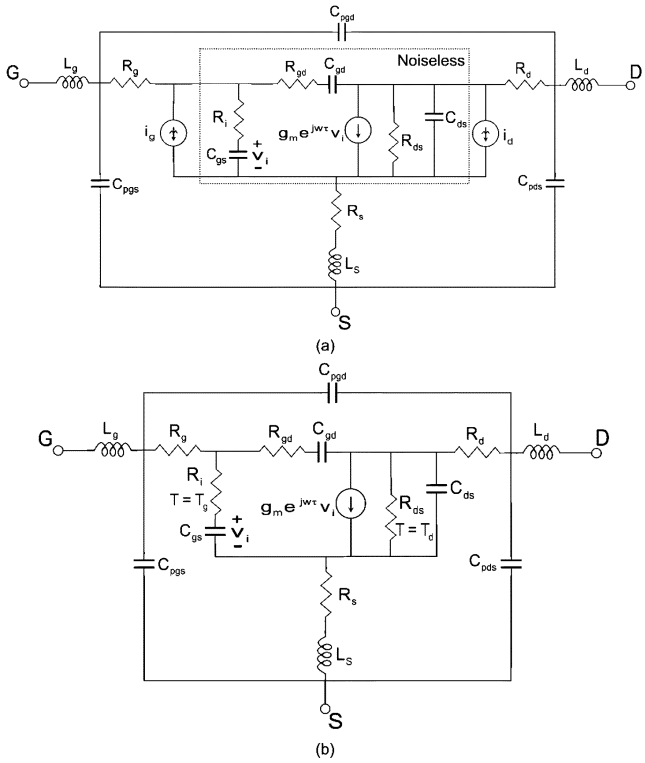

Fig. 8. Small-signal model including noise modeling for: (a) van der Ziel method; the intrinsic model is noiseless while the extrinsic parasitics still generate noise and (b) Pospieszalski method; only the channel and drain–source resistances generate noise.

Comparing both, one sees that both work well at predicting the $\rm Nf_{min}$ and optimum source reflection-coefficient magnitude. Pospieszalski's model has trouble predicting the phase of the reflection coefficient, while the van der Ziel model has difficulties with the noise resistance. It is worth mentioning that a correlation of a magnitude of 0.8 was predicted here at 5 GHz, as well as in the paper Lee *et al.* [28]. An assumption of the Pospieszalski model is that the noise sources are uncorrelated. We see this is not always the case. For frequencies well above 10 GHz, and small gate-length devices (0.25 μm or less), the correlation might well be close to 1. If the correlation is not 1, though, the Pospieszalski model may give predictions that are not true to the physics of the device. It should also be pointed out that the Pospieszalski model has described in it a limitation given by the inequality

$$1 \leq \frac{4R_n}{(F_{\rm min}-1)R_{\rm opt}} < 2 \tag{4}$$

with R_n being the unnormalized noise resistance and $R_{\rm opt}$ being the real part of the optimum source impedance. This condition was not met in the modeling above, despite the accuracy of the results.

VI. Conclusion

It has been shown that, against frequency and current, the $\rm Nf_{min}$ for AlGaN/GaN HEMTs does not change with aluminum composition in the barrier. This leaves a free variable when designing a device for noise. Other measurements showed, for the

first time, that at higher currents, a device with a thin AlN layer will have slightly lower noise than does a device without the layer. However, a device with a thin AlN layer can have the same noise as a device without the layer if both devices are biased for best noise performance. This is useful if a design goal for an X-band low-noise amplifier (LNA) was to have slightly more power, yet still maintain the same specification on noise figure. These two studies, and the performance seen from In channel devices, as seen in Table I, might suggest that it is the channel material that determines the noise performance. Finally, the Pospieszalski and van der Ziel models were applied to six different devices showing the strengths and limitations of each.

ACKNOWLEDGMENT

The authors would like to thank the Office of Naval Research for their continued support of GaN projects at the University of California at Santa Barbara (UCSB). The authors would also like to thank R. Wallace, Maury Microwave, Ontario, CA, for numerous debugging conversations of our source–pull noise figure system.

REFERENCES

[1] W. Lu, V. Kumar, R. Schwindt, E. Piner, and I. Adesida, "DC, RF, and microwave noise performance of AlGaN/GaN HEMTs on aluminum concentration," *IEEE Trans. Electron Devices*, vol. 50, no. 4, pp. 2499–2503, Apr. 2003.

[2] J. S. Moon, M. Micovic, A. Kurdoghlian, P. Janke, P. Hashimoto, W.-S. Wong, L. McCray, and C. Nguyen, "Microwave noise performance of AlGaN–GaN HEMTs with small DC power dissipation," *IEEE Electron Device Lett.*, vol. 23, no. 11, pp. 637–639, Nov. 2002.

[3] W. Lu, V. Kumar, R. Schwindt, E. Piner, and I. Adesida, "DC, RF, and microwave noise performance of AlGaN/GaN HEMTs on sapphire substrates," *IEEE Trans. Microw. Theory Tech.*, vol. 50, no. 11, pp. 2499–2503, Nov. 2002.

[4] A. Chini, D. Buttari, R. Coffie, S. Heikman, S. Keller, and U. K. Mishra, "12 W/mm power density AlGaN/GaN HEMTs on sapphire substrate," *IEEE Electron. Lett.*, vol. 40, no. 1, pp. 73–74, Jan. 2004.

[5] A. T. Ping, E. Piner, J. Redwing, M. A. Khan, and I. Adesida, "Microwave noise performance of AlGaN/GaN HEMTs," *Electron. Lett.*, vol. 36, pp. 175–176, Jan. 2000.

[6] N. X. Nguyen, M. Micovic, W.-S. Wong, P. Hashimoto, P. Janke, D. Harvey, and C. Nguyen, "Robust low microwave noise GaN MODFETs with 0.6 dB noise figure at 10 GHz," *IEEE Electron. Lett.*, vol. 36, no. 3, pp. 469–471, Mar. 2000.

[7] J.-W. Lee, V. Kumar, R. Schwindt, A. Kuliev, R. Birkhahn, D. Gotthold, and S. Guo, "Microwave noise performances of AlGaN/GaN HEMT's on semi-insulating 6H-SiC substrates," *Electron. Lett.*, vol. 40, pp. 80–81, Jan. 2004.

[8] S. S. H. Hsu and D. Pavlidis, "Low noise AlGaN/GaN MODFET's with high breakdown and power characteristics," in *23rd Annu. Gallium Arsenide Integrated Circuit Symp. Tech. Dig.*, Oct. 2001, pp. 229–232.

[9] J. Mateos, D. Pardo, T. González, P. Tadyszak, F. Danneville, and A. Cappy, "Influence of Al mole fraction on the noise performance of GaAs/$Al_xGa_{1-x}As$ HEMT's," *IEEE Trans. Electron Devices*, vol. 45, no. 9, pp. 2081–2083, Sep. 1998.

[10] H. Kawasaki, T. Shino, M. Kawano, and K. Kamei, "Super low noise AlGaAs/GaAs HEMT with one tenth micron gate," in *IEEE MTT-S Int. Microwave Symp. Dig.*, Jun. 13–15, 1989, pp. 423–426.

[11] J.-H. Lee, H.-S. Yoon, C.-S. Park, and P. Hyung-Moo, "Ultra low noise characteristics of AlGaAs/InGaAs/GaAs pseudomorphic HEMT's with wide head T-shaped gate," *IEEE Electron Device Lett.*, vol. 16, no. 6, pp. 271–273, Jun. 1995.

[12] C. S. Whelan, P. F. Marsh, W. E. Hoke, R. A. McTaggart, C. P. McCarroll, and T. E. Kazior, "GaAs metamorphic HEMT (MHEMT): An attractive alternative to InP HEMT's for high performance low noise and power applications," in *Proc. Indium Phosphide and Related Materials Conf.*, May 14–18, 2000, pp. 337–340.

[13] H. Rohdin, A. Nagy, V. Robbins, C. Su, C. Madden, A. Wakita, J. Raggio, and J. Seeger, "Low-noise high-speed $Ga_{.47}In_{.53}As/Al_{.48}In_{.52}As$ 0.1-μm MODFETS and high-gain/bandwidth three-stage amplifier fabricated on GaAs substrate," presented at the 7th Int. Indium Phosphide and Related Materials Conf., May 1995.

[14] M.-Y. Kao, K. H. G. Duh, P. Ho, and P.-C. Chao, "An extremely low-noise InP-based HEMT with silicon nitride passivation," in *Int. Electron Devices Meeting Tech. Dig.*, Dec. 11–14, 1994, pp. 907–910.

[15] Y. Ando, A. Cappy, K. Marubashi, K. Onda, H. Miyamoto, and M. Kuzuhara, "Noise parameter modeling for InP-based pseudomorphic HEMTs," *IEEE Trans. Electron Devices*, vol. 44, pp. 1367–1374, Sep. 1997.

[16] H. C. Duran, B.-U. H. Klepser, and W. Bachtold, "Low-noise properties of dry gate recess etched InP HEMT's," *IEEE Electron Device Lett.*, vol. 17, no. 10, pp. 482–484, Oct. 1996.

[17] F. Aniel, M. Enciso-Aguilar, L. Giguerre, P. Crozat, R. Adde, T. Mack, U. Seiler, T. Hackbarth, H. Herzog, U. Konig, and B. Raynor, "High performance 100 nm T-gate strained $Si/Si_{0.6}Ge_{0.4}$ n-MODFET," presented at the Elsevier Solid-State Electronics Conf., Feb. 2003.

[18] L. Shen, S. Heikman, B. Moran, R. Coffie, N.-Q. Zhang, D. Buttair, P. Smorchkova, S. Keller, S. P. DenBaars, and U. K. Mishra, "AlGaN/AlN/GaN high-power microwave HEMT," *IEEE Electron Device Lett.*, vol. 22, no. 10, pp. 457–459, Oct. 2001.

[19] P. H. Ladbrooke, *MMIC Design: GaAs FET's and HEMTs*. Boston, MA: Artech House, 1989.

[20] H. Rothe and W. Dahlke, "Theory of noisy fourpoles," in *Proc. IRE*, vol. 44, Jun. 1956, pp. 811–818.

[21] M. Berroth and R. Bosch, "Broad-band determination of the FET small-signal equivalent circuit," *IEEE Trans. Microw. Theory Tech.*, vol. 38, no. 7, pp. 891–895, Jul. 1990.

[22] G. Dambrine, A. Cappy, F. Heliodore, and E. Playez, "A new method for determining the FET small-signal equivalent circuit," *IEEE Trans. Microw. Theory Tech.*, vol. 36, no. 7, pp. 1151–1159, Jul. 1988.

[23] H. Morkoç and L. Lianghong, "GaN-based modulation-doped FET's and heterojunction bipolar transistors," in *Nitride Semiconductors: Handbook on Materials and Devices*, P. Ruterana, M. Albrecht, and J. Neugebauer, Eds. Berlin, Germany: Wiley-VCH, 2003, pp. 608–613.

[24] R. A. Pucel, H. A. Haus, and H. Statz, "Signal and noise properties of gallium arsenide microwave field-effect transistors," *Adv. Electron. Electron Phys.*, vol. 38, pp. 195–265, 1975.

[25] A. Van Der Ziel, "Gate noise in field effect transistors at moderately high frequencies," *Proc. IEEE*, vol. 51, no. 3, pp. 461–467, Mar. 1963.

[26] H. Hillbrand and P. Russer, "An efficient method for computer-aided noise analysis of linear amplifier networks," *IEEE Trans. Circuits Syst.*, vol. CAS-23, no. 4, pp. 235–238, Apr. 1976.

[27] S. Lee, V. Tilak, K. J. Webb, and L. Eastman, "Intrinsic noise characteristics of AlGaN/GaN HEMTs," in *IEEE MTT-S Int. Microwave Symp. Dig.*, vol. 3, Jun. 2002, pp. 1415–1418.

[28] S. Lee, K. J. Webb, V. Tilak, and L. Eastman, "Intrinsic noise equivalent-circuit parameters for AlGaN/GaN HEMTs," *IEEE Trans. Microw. Theory Tech.*, vol. 51, no. 5, pp. 1567–1577, May 2003.

[29] M. W. Pospiezalski, "Modeling of noise parameters of MESFET's and MODFET's and their frequency and temperature dependence," *IEEE Trans. Microw. Theory Tech.*, vol. 37, no. 9, pp. 1340–1350, Sep. 1989.

Christopher Sanabria (S'98) was born in Pasadena, TX, in 1979. He received the B.S. degree in electrical engineering from the University of Notre Dame, Notre Dame, IN, in 2001, the M.S. degree from the University of California at Santa Barbara (UCSB), in 2002, and is currently working toward the Ph.D. degree at UCSB.

He has served internships with Delphi-Delco Electronics during the summers of 1998 and 1999, Texas Instruments Incorporated during the summer of 2000, and Agilent Laboratories, Agilent Technologies during the summer of 2003. His research interests include modeling and measurements of GaN HEMTs and analog circuits for noise and power applications.

Hongtao Xu (S'03) received the B.S. degree in electronic engineering from Fudan University, Shanghai, China, in 1997, the M.S. degree in electrical engineering from the University of California at Santa Barbara (UCSB), in 2001, and is currently working toward the Ph.D. degree at UCSB.

His research interests include design and fabrication of power amplifiers, LNAs, and oscillators in GaN-based HEMT technology.

Tomás Palacios (S'99) received the Telecommunication Engineering degree from the Polytechnic University of Madrid, Madrid, Spain, in 2001, and is currently working toward the Ph.D. degree in electrical engineering at the University of California at Santa Barbara (UCSB).

Since 1998, he has been involved with GaN-based devices, initially with the Institute for Systems based on Optoelectronics and Microtechnology (ISOM), in Madrid, Spain, and since 2002, with UCSB. During the summer of 2000, he was a Visiting Scholar with the Microelectronic Group, European Organization for Nuclear Research (CERN). His current research interest focuses on the search of novel GaN-based transistors for millimeter-wave applications. He has authored or coauthored over 45 papers concerning semiconductor devices in international journals and conferences.

Arpan Chakraborty was born in Calcutta, India, in 1977. He received the B.Sc. degree in physics from the University of Calcutta, Calcutta, India, in 1999, the M.S. degree in physical sciences from the Indian Institute of Science, Bangalore, India, in 2002, and is currently working toward the Ph.D. degree in electrical and computer engineering at the University of California at Santa Barbara (UCSB).

His research interests includes MOCVD growth and characterization of group-III nitrides for electronic and opto-electronic applications.

Sten Heikman received the Civilingenjör degree in applied physics and electrical engineering from Linköping University, Linköping, Sweden, in 1998, the M.S. degree in electrical and computer engineering from the University of Massachusetts at Amherst, in 1998, and the Ph.D. degree in electrical and computer engineering from the University of California at Santa Barbara (UCSB), in 2002.

He is currently with the Department of Electrical and Computer Engineering, UCSB, where he conducts research on various aspects of group-III nitride semiconductors, including field-effect transistor (FET) structures and epitaxial growth techniques.

Umesh K. Mishra (S'80–M'83–SM'90–F'95) received the B.Tech. from the Indian Institute of Technology (IIT) Kanpur, India, in 1979, the M.S. degree from Lehigh University, Bethlehem, PA in 1980, and the Ph.D. degree from Cornell University, Ithaca, NY, in 1984, all in electrical engineering.

He has been with various laboratory and academic institutions, including Hughes Research Laboratories, Malibu, CA, The University of Michigan at Ann Arbor, and General Electric, Syracuse, NY, where he has made major contributions to the development of AlInAs–GaInAs HEMTs and HBTs. He is currently a Professor and the Department Chair at the Department of Electrical and Computer Engineering, University of California at Santa Barbara (UCSB). He has authored or coauthored over 450 papers in technical journals and conferences. He holds nine patents. His current research interests are in oxide-based III–V electronics and III–V nitride electronics and opto-electronics.

Dr. Mishra was a corecipient of the Hyland Patent Award presented by Hughes Aircraft and the Young Scientist Award presented at the International Symposium on GaAs and Related Compounds.

Robert A. York (S'85–M'89–SM'99) received the B.S. degree in electrical engineering from the University of New Hampshire, Durham, in 1987, and the M.S. and Ph.D. degrees in electrical engineering from Cornell University, Ithaca, NY, in 1989 and 1991, respectively.

He is currently a Professor of electrical and computer engineering with the University of California at Santa Barbara (UCSB), where his group is currently involved with the design and fabrication of novel microwave and millimeter-wave circuits, high-power microwave and millimeter-wave amplifiers using spatial combining and wide-bandgap semiconductor devices, and application of ferroelectric materials to microwave and millimeter-wave circuits and systems.

Dr. York was the recipient of the 1993 Army Research Office Young Investigator Award and the 1996 Office of Naval Research Young Investigator Award.